Jpn. J. Appl. Phys. Vol. 35 (1996) pp. 2318–2325
Part 1, No. 4A, April 1996

Effects of Atomic Arrangement at Tip Apex and Tip-Sample Distance on Atomic Force Microscopy Images: A Simulation Study

Masaharu KOMIYAMA, Shin'ya OHKUBO[1], Katsuyuki TAZAWA[1], Kazuya TSUJIMICHI[1], Akiyasu HIROTANI[1], Momoji KUBO[1] and Akira MIYAMOTO[1]

Department of Chemistry, Yamanashi University, Takeda, Kofu 400, Japan
[1]*Department of Molecular Chemistry and Engineering, Tohoku University, Sendai 980–77, Japan*

(Received August 29, 1995; accepted for publication January 16, 1996)

Using a newly developed atomic force microscopy (AFM) simulator ACCESS (AFM simulation code for calculating and evaluating surface structures), effects of the atomic arrangement at the tip apex and tip-sample distance on AFM image resolution were examined. A tip which has an atom protruding at its apex and is scanning in the repulsive force range is found to be necessary for obtaining atomically resolved AFM images. The second atomic layer of the tip determines the force characteristics of the system, as well as the AFM image phase shift. Since in actual AFM systems these two effects are convoluted, it is apparent that scanning under the same applied force does not necessarily mean the same tip-sample distance or the same image resolution, unless one is sure that the atomic arrangement at the proximity of the tip apex is the same. It is also found that surface point defects mirror the atomic arrangements of the tip apex in the AFM images, both in attractive and repulsive force ranges, indicating their possible use in tip apex evaluation at the atomic level.

KEYWORDS: atomic force microscopy, tip apex geometry, simulation, Morse potential, point defects, resolution limit, contact mode, noncontact mode, attractive force, tip-sample distance

1. Introduction

Since the advent of atomic force microscopy (AFM)[1)] and the achievement of atomic resolution on insulator surfaces,[2)] applications of AFM are rapidly expanding in diverse fields such as material sciences, electrochemistry and biology.[3)]

A large number of AFMs are operated in the static-contact mode, in which the AFM tip scans the sample surface in the repulsive force range under a constant applied force. While this operating mode produces stable and reproducible atomic images for mica and other "hard" surfaces, "soft" samples such as porous thin films and biological materials are sometimes damaged under this imaging mode. This led to the development of a dynamic-contact or tapping mode, which still images the surface in the repulsive force range but with the tip vibrating in the z-direction; hence the tip does not drag or scratch the sample surface. Recent efforts are being made to operate an AFM in the attractive force range[4)] with both static and dynamic modes. Since the attractive force range exists farther from the surface compared to the repulsive force range, this means a long tip-sample distance and hence weaker force variation to be detected.

Despite its practical importance and widespread use, the AFM imaging mechanism has not yet been clarified, and the effects on AFM images of parameters such as tip-sample distances (i.e., force variation along the surface normal) and tip apex geometries have not been extensively studied. There are several reasons for the lack of studies on such basic points. One of them may be that, unlike scanning tunneling microscopy (STM), it is not easy to estimate tip-sample distances in AFM. This is due to the fact that forces exerted by the sample atoms on the tip consist of not only one but several components,[4,5)] including atomic, electrostatic (Coulomb), dipole, dispersion (van der Waals) and other "chemical" forces such as hydrophobic force. The shapes of those force curves are expected to differ markedly; thus it is not possible to determine the tip-sample distance experimentally by simply taking the AFM force curve.

The other source of complexity is that, again unlike STM, it is not possible to determine experimentally the geometrical arrangement of the apex atoms of the AFM tip. Thus it is sometimes difficult to separate the tip artifacts from actual surface properties, leaving the interpretation of atomic-level AFM images and force characteristics often ambiguous and inconclusive.

One way of addressing these problems is the use of atomistic simulations. Several attempts have been made, although most of them are concerned with tip-sample interactions,[6–15)] and examinations through the simulations of AFM images themselves are scarce.[16–25)] Furthermore, most of those latter works deal with imaging in the repulsive force range that corresponds to the contact-mode AFM operation, and imaging in the attractive force range (noncontact mode) has not been studied in detail. In addition, most of these works employ only one tip geometry, and the effects of tip geometries on AFM images and force characteristics have not been well explored.

Here we report the development of an AFM simulator ACCESS (AFM simulation code for calculating and evaluating surface structures) and its visualization tool VITAMIN 95 (visualization tool for atomic force microscopy nineteen ninety-five). Using these programs, the image and the force variations along the sample surface normal as functions of the crystallographic structure of the tip and tip apex geometries were examined.

2. Methods

The newly developed AFM simulator ACCESS calculates pairwise forces acting between the atoms in the AFM tip and those in the sample surface, and determines the total forces acting on the tip. The simulator is made flexible so that it can adapt various types of pairwise po-

tentials including Coulomb potential, and can also incorporate the molecular dynamics (MD) method.[25] It can produce a force field map on the sample surface (corresponding to constant-height or deflection-mode image) or a z-position map of the tip necessary to keep the force acting on the tip constant (corresponding to constant-force mode image) as the tip scans the surface. It is also possible to calculate the lateral force distribution as the tip scans the surface, thus simulating lateral force microscopy (LFM).[25] The obtained images are visualized using VITAMIN 95. In the present study ACCESS and VITAMIN 95 were installed and run on a Hewlett-Packard 9000 Model-712/60 engineering workstation.

Model AFM systems consisting of Fe metal or diamond cluster tips and a Cu(100) surface were examined. The use of single-component tips and a metal sample as model systems simplifies the forces acting between the tip and the sample compared to multicomponent and thus (partially) ionic systems.

The model sample surface examined, which consists of 4 atomic layers of Cu(100), is shown in Fig. 1(a). In order to avoid edge effects that may affect the calculated results, an area of 5×5 surface unit cells under two-dimensional periodic boundary conditions was scanned. One of the examined surfaces is crystallographically perfect (Fig. 1(b)), another has a point defect at the center (c) and yet another has a monoatomic step across it (d).

A tip made of iron (bcc structure) or diamond (diamond structure) was used as the model AFM tip. Any other single-component materials may also be used for the present purpose. Preliminary simulation results using a single iron atom as the AFM tip have already been reported.[23] While this single-atom tip represents "the most ideal" tip for AFM measurements, it is not easily realized in actual situations, thus the present study uses more realistic tip geometries. Several types of tips were constructed as shown in Fig. 2. Figures 2(a) and 2(b) are pyramid-shaped clusters with the apex atoms pointing down toward the sample surface. Tip (a) consists of 30 iron atoms and surrounded by four of its {110} faces and tip (b) consists of 55 carbon atoms surrounded by three of its {111} faces. Figures 2(c) and 2(d) are flat tips, (c) being a three-layered iron slab of 2×2 (100) facing toward the sample and (d) being a two-layered diamond slab with seven-atom, sixfold (111) facing toward the sample surface. An iron tip with an adatom on a 3×3 (100) surface (Fig. 2(e)) was also examined. Throughout this paper those tips are referred to with notations (a) through (e) found in Fig. 2.

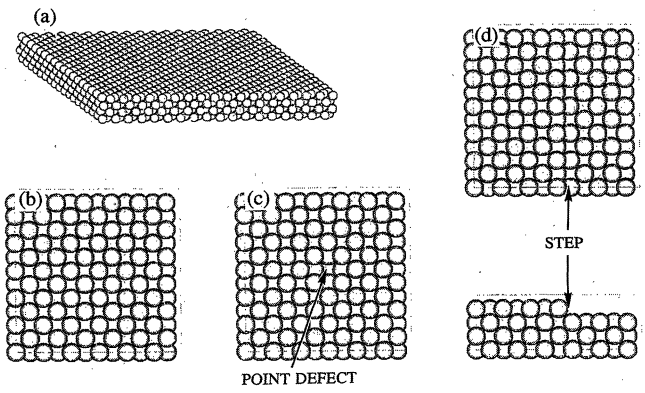

Fig. 1. The model sample surface (a) and top views of scanned area of perfect (b), point defect (c) and stepped (d) surfaces.

Forces acting between the atoms in the tip and those in the sample were calculated using the following Morse-type potential (1).

$$U_{ij}(r_{ij}) = D_{ij}[\exp\{-2\beta_{ij}(r_{ij} - r^*_{ij})\} - 2\exp\{-\beta_{ij}(r_{ij} - r^*_{ij})\}] \quad (1)$$

Here D_{ij} denotes bond energy, β_{ij} shape of potential curve, r_{ij} distance and r^*_{ij} average distance between atoms i and j. The forces involved in actual AFM systems may be diverse,[4,5] and thus the present potential is only an example and is not meant to cover all the possible potentials existing in actual AFM systems. The use of Morse potential, instead of other potentials such as Lennard–Jones (L–J), is purely for convenience. However, as discussed below, the qualitative features of the present simulation results depend very weakly on large parameter changes of the Morse potential. This also implies that the use of other potentials having similar shape, such as L–J, results in qualitatively similar results as those presented here.

A potential curve and its derivative, the force curve, for an iron-copper system are shown in Fig. 3. The Morse parameter values are listed in Table I. For Fe–Cu pairs, the Morse parameter values for pure components were taken from literature.[26] Their geometrical mean is used for $D_{\text{Cu-Fe}}$ and $\beta_{\text{Cu-Fe}}$, and arithmetic mean for $r^*_{\text{Cu-Fe}}$. For C–Cu pairs there exist no literature values for pure C; thus we used typical Morse parameter values for $D_{\text{Cu-C}}$ and $\beta_{\text{Cu-C}}$, while $r^*_{\text{Cu-C}}$ is determined from their van der Waals radii. In order to examine the parameter dependence of the present simulation results, we also simulated the entire cases of Fe–Cu system presented here with parameter values employed in our previous study,[23] and found that there exists no difference in the qualitative features of the simulated results, indicating a very weak

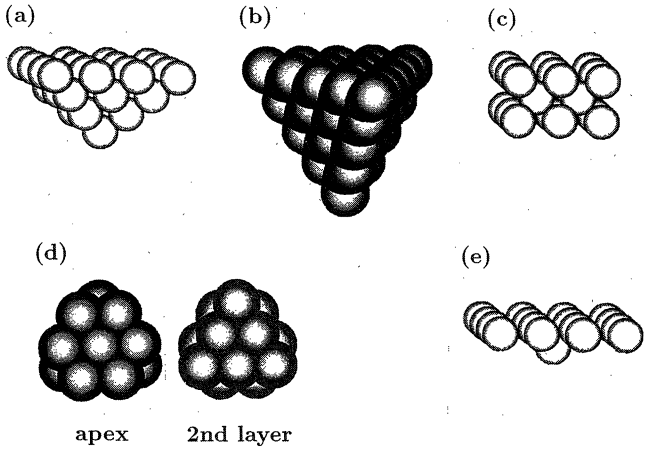

Fig. 2. The examined geometries of AFM tips: pyramids made of iron (a) and diamond (b), flat tips made of 2×2 unit cells of iron (100) (c) and 7-atom diamond (111) (d) and iron adatom on iron (100) (e). The second layer of the tip (d) is also shown.

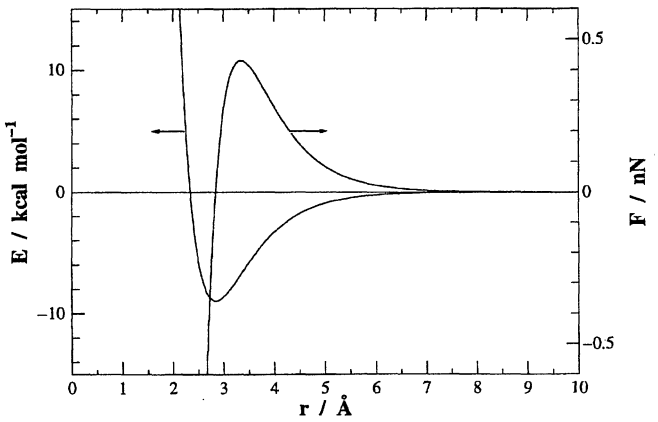

Fig. 3. A Morse-type potential and its force curve for an iron-copper system. r is the distance, E the bond energy and F the force between Fe and Cu atoms.

Table I. Morse potential parameters used in the present study.

	D_{ij} (kcal/mol)	β_{ij} (1/Å)	r^*_{ij} (Å)
Fe–Cu	8.72	1.37	2.86
C–Cu	3.00	1.98	2.98

Table II. Tip-sample distances employed in the present constant-height AFM simulations.

	Repulsive	Strongly attractive	Weakly attractive
Fe–Cu	0.65	3.36	4.86
C–Cu	1.67	3.34	3.98

dependence of the present results on the Morse parameter values.

Actual calculations were performed as follows. Using eq. (1), the z-component of the force exerted by each atom in the sample on each atom in the tip was calculated, and their sum was taken as the total force on the tip in the z direction at that tip position. This was repeated for each tip position as it scans the surface, and the contour map of the force field felt by the tip was obtained. The force image thus produced corresponds to the constant-height (deflection) image in actual AFM measurements. For the constant-force image simulations, the tip position was adjusted so that the total force on the tip equals a set value, and then the tip-sample distance was recorded.

For constant-height imaging, three tip-sample distances, which are defined as the nucleus-nucleus distances between the topmost atomic layer of the sample and the tip apex atom, were selected and are shown in Table II. Those values were chosen so that the tips are either (1) in the repulsive force range (termed "repulsive"), (2) at a distance where attractive force is strongest ("strongly attractive") or (3) far from the surface where attractive force is weak ("weakly attractive").

3. Results and Discussion

3.1 *Constant-force mode vs. constant-height mode*

Two scanning modes are often employed in actual AFM measurements: constant-force mode with z-position feedback and constant-height mode without or under very slow z-position feedback. The latter is also called a deflection mode. Comparison of the simulated AFM images using the iron and diamond pyramid tips (Figs. 2(a) and 2(b)) indicated that both tips give essentially the same images, indicating a rather weak tip structure dependence. It turned out, as discussed later, that this is due to the fact that for both tips the second atomic layer has a high symmetry around the z-axis of the tip. Thus both scanning modes are compared here with the pyramid iron tip and shown in Fig. 4.

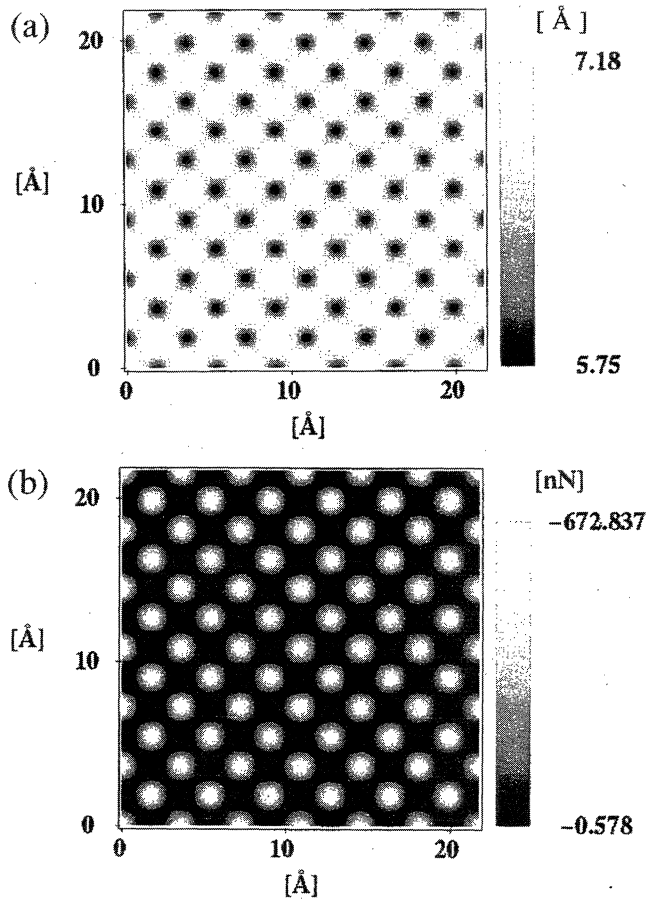

Fig. 4. Simulated constant-force image (a), taken with an applied force of −10 nN (repulsive), and simulated deflection-mode image (b) taken at a repulsive tip-sample distance of 1.67 Å, both using a pyramid diamond tip.

The constant-force image (a) in Fig. 4, which was taken with an applied force of −10 nN (repulsive force range), shows perfect atomic resolution. It is interesting to note that with these scanning conditions, the observed metal atom corrugation amounts to approximately 1.4 Å, which is one order of magnitude larger than that observed with STM. In STM metal atom corrugations are very small because of the delocalization of conduction band electrons, and Fig. 4(a) tells us that for such a system AFM may possess a resolution advantage over STM. In the deflection-mode image (b) taken in the repulsive force range the force variation on this surface at this tip-sample distance exceeds 600 nN, which is due to the rather short tip-sample distance examined here.

Comparison of the two scanning mode images indi-

cates that there appears to exist no essential difference between the two modes in the present simulations. This is also true for the attractive force scanning and for other surfaces studied here. The lack of difference between the two mode images found in Fig. 4 reflects the fact that the present simulation does not take into account any transient factors that may be associated with actual AFM measurements. Thus despite the above results, we do not claim the triviality in the choice of scanning modes in practice. In actual AFM measurements these two modes may involve different electronic and/or mechanical circuits, and their differences manifest themselves in the differences in scanning stability, noise level, data resolution, and scanning rates. Thus in actual AFM measurements the choice of the scanning mode may be based on these considerations. Throughout the present study, however, the constant-height mode is mostly employed, mainly for its short computational time.

3.2 *Force variations along the surface normal: pyramid tip geometry*

Force variations along the sample surface normal are examined using an iron pyramid tip (Fig. 2(b)). It is noted again that the diamond pyramid tip gives essentially the same results with the iron tip. The simulated results on perfect and point-defect Cu(100) model surfaces (Figs. 1(b) and 1(c)) are shown in Figs. 5 and 6, respectively, as a function of tip-sample distance.

It is found that the results obtained with pyramid-shaped tip almost exactly parallel the results obtained using a single-atom tip.[23] For the perfect sample surface, repulsive scanning that corresponds to the contact-mode imaging in actual AFM operation gives a perfectly atom-resolved image (Fig. 5(a)). When the scanning is performed at attractive force distances, contrast inversions were observed as in the case of the single-atom tip.[23] At a strongly attractive distance, the stronger attractive force (lighter tone) in Fig. 5(b) is not located above the atom position any more, but is located at the center of each square made of four Cu atoms. This is due to the fact that at this tip-sample distance, the composite force from a collection of atoms becomes stronger than the force from a single atom. The composite force originates from the four atoms that form a surface unit cell.

Second contrast inversion is observed when the tip-sample distance is increased to a weakly attractive position as shown in Fig. 5(c). Now the bright spots (stronger attractive force) return to the surface atomic locations again, although this is not an atom-resolved image any more. This happens in the present case because the examined surface has fourfold symmetry and the used potential is spherical, and thus the composite force gives exactly the same periodicity as the sample surface. Thus the correspondence between the surface atom positions and the bright spots is purely coincidental. On the other hand, this correspondence tells us that if such a condition is realized in actual AFM measurements, one may observe an apparently "atomically resolved" image even though it does not reflect true atomic locations.

As in the case of the single-atom tip,[23] simulations on a point-defect surface show the above-discussed points

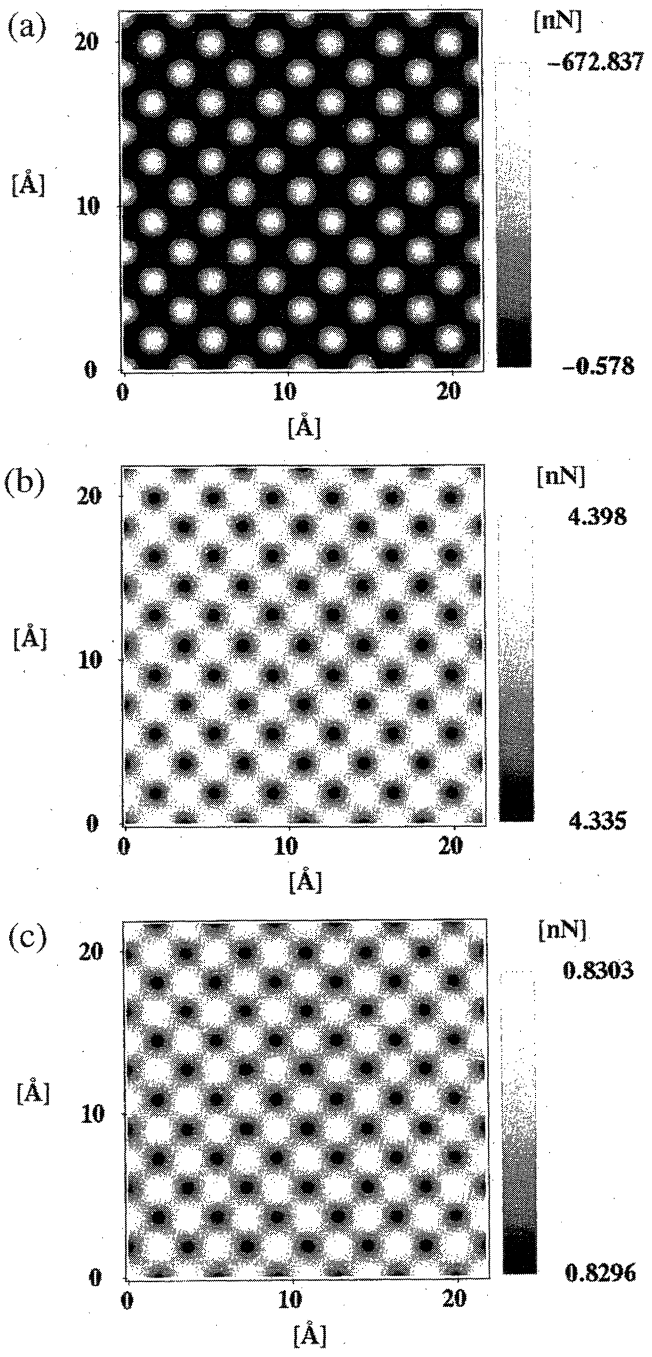

Fig. 5. Simulated constant-height AFM images of a perfect Cu(100) surface (Fig. 1(b)) using a pyramid-shaped iron tip. Tip is at (a) repulsive, (b) strongly attractive and (c) weakly attractive force distance.

more clearly, as found in Fig. 6. At a repulsive force distance (Fig. 6(a)), the defect location as well as atom locations is precisely reproduced as expected. At attractive force distances (Figs. 6(b) and 6(c)), the defect image is blurred, and the extent of blurring indicates the range of the force that is exerted on the tip at a specific tip position. Thus in Fig. 6(b) which is scanned at a strongly attractive distance, four bright spots surrounding the point defect lose their resolution, indicating that the collective force which produces one bright spot comes from about four atoms that consist a surface unit cell. The results at a weakly attractive distance appears to be almost the

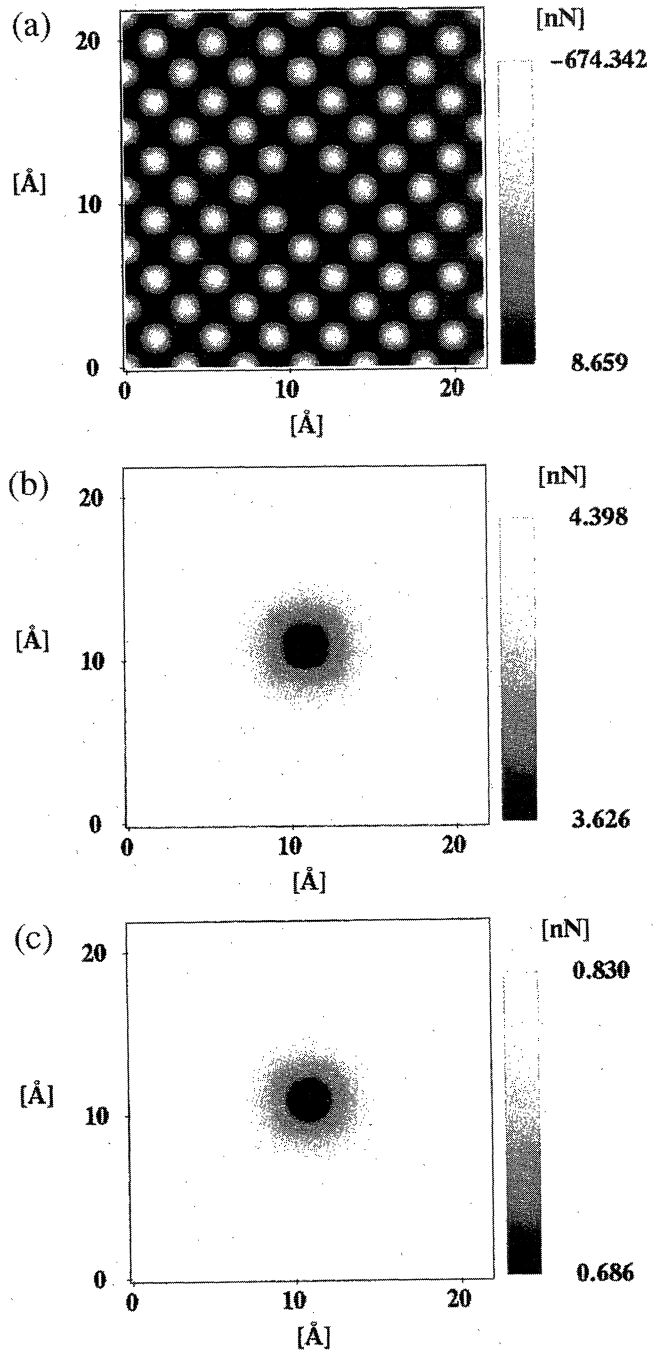

Fig. 6. Simulated constant-height AFM images of a point-defect Cu(100) surface (Fig. 1(c)) using a pyramid-shaped iron tip. Tip is at (a) repulsive, (b) strongly attractive and (c) weakly attractive force distance.

same as the one at a strongly attractive distance. This slightly differs from the case of the single-atom tip,[23] in which 8 atoms surrounding the point defect becomes indistinguishable at this distance. The difference is attributed to the presence of the second atomic layer in the present pyramid tip. The above considerations on the point defect surface strongly indicate that in the apparently perfect surface images found in Figs. 5(b) and 5(c) true atomic resolution is not achieved, although it may appear to be so.

3.3 *Effect of the second atomic layer of the tip*

The fact that the results obtained using a single-atom tip and a pyramid-shaped tip are almost exactly parallel each other indicates that the AFM image resolution is mainly determined by the apex atom, and the contribution to resolution from other parts of the tip is not significant within the framework of the present calculations. This conclusion may be confirmed by examining the adatom tip geometry (Fig. 2(e)). It turned out that the iron adatom tip also gave essentially the same results as those of the iron single-atom and pyramid tips, thus confirming the above conclusion.

It is found, however, that the total force exerted on the tips varies markedly. Table III compares the maximum force felt by these three an-atom-at-the-apex tips made of iron. For comparison, simulations presented in this section are calculated using the Morse parameters used in our previous paper,[23] *viz.*, $D_{ij} = 3.0$ kcal/mol, $\beta_{ij} = 1.98$ Å and $r^*_{ij} = 2.52$ Å. The tip-sample distances also follow those of the previous paper. At the attractive force distances (columns 3 and 4), the single-atom tip feels the weakest surface force, the pyramid tip the next and the adatom tip the strongest. This is apparently due to the contribution from the second atomic layer of the tip apex. The single-atom tip has no second layer contribution, and the difference between the pyramid and the adatom tips comes from the difference in the number of atoms in the second layer: four for pyramid and 16 for adatom. When the apex atom is in the repulsive distance, however, the second layer atoms are in the attractive force range, and they reduce the total repulsive force. Thus in column 2 of Table III total repulsive force decreases from single-atom to pyramid to adatom tips.

Actual AFM systems may not be as simple as this: various forces with various ranges may exist, and depending on their ranges the atomic layers involved in determining the total force may vary. Nevertheless, from the above discussion it became clear that two factors are important when considering the effect of AFM tip structures on AFM images: one factor is the tip apex geometry which governs the image resolution, and the other is the size of the second atomic layer and up which governs the force characteristics. The latter may be considered as the effect of the tip apex curvature instead, since the local curvature at the tip apex may be determined largely by the first and subsequent atomic layers at the apex.

3.4 *Force variations along the surface normal: flat tip geometry*

In the case of flat tip geometry, iron and diamond show

Table III. Maximum force values felt by various an-atom-at-the-apex tips made of iron.

Tip shape	Repulsive	Strongly attractive	Weakly attractive
Single-atom	−51 nN	0.46 nN	0.19 nN
Pyramid	−48 nN	0.71 nN	0.27 nN
Adatom	−43 nN	1.28 nN	0.45 nN

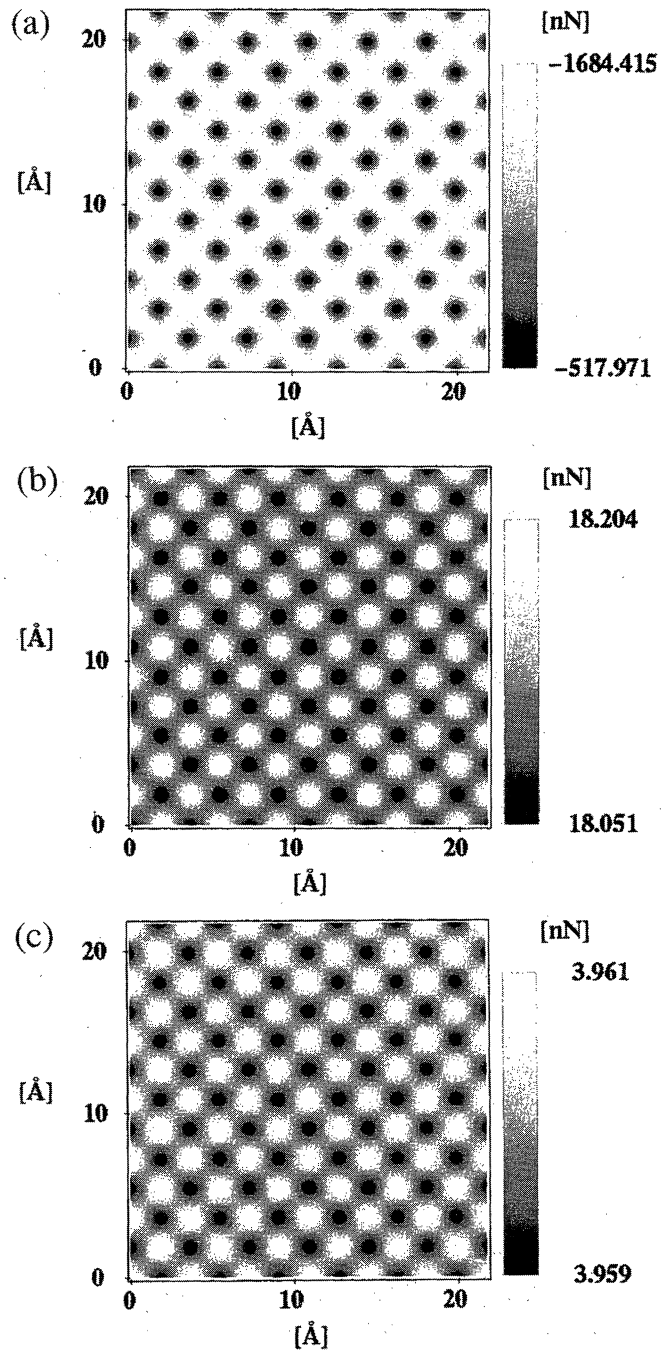

Fig. 7. Simulated constant-height AFM images of a perfect Cu(100) surface (Fig. 1(b)) using a flat iron tip. Tip is at (a) repulsive, (b) strongly attractive and (c) weakly attractive force distance.

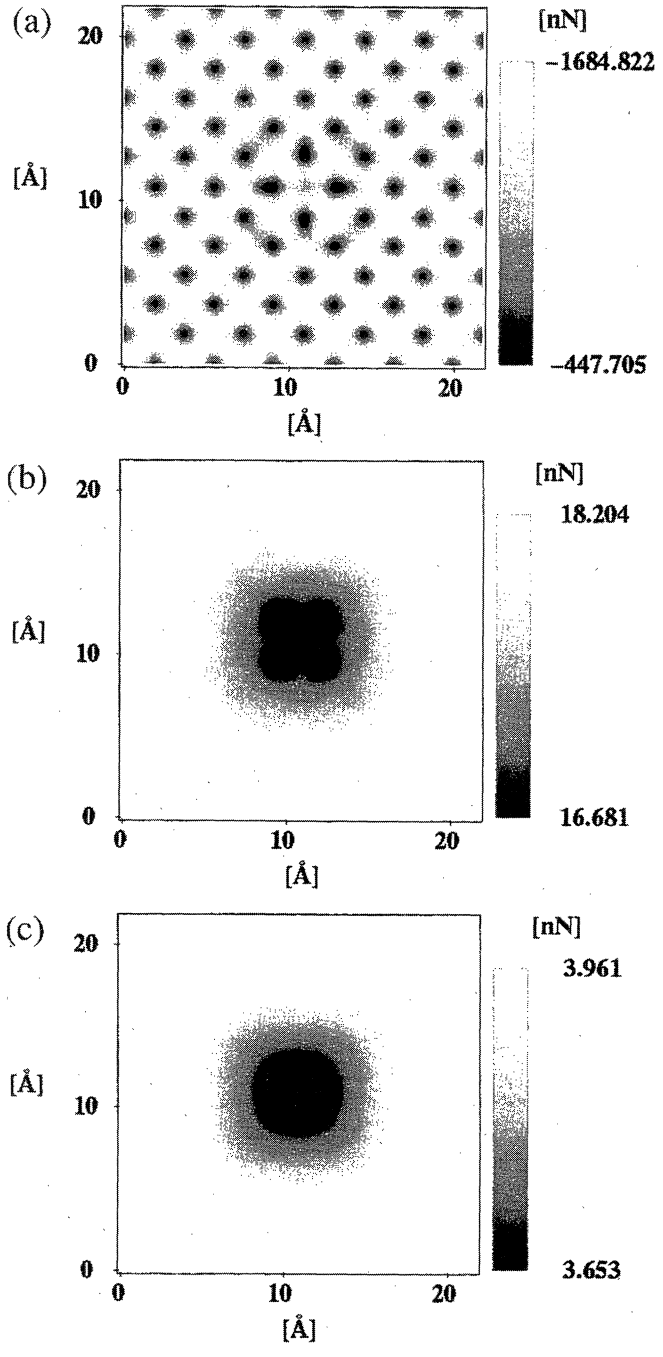

Fig. 8. Simulated constant-height AFM images of a point defect Cu(100) surface (Fig. 1(c)) using a flat iron tip. Tip is at (a) repulsive, (b) strongly attractive and (c) weakly attractive force distance.

distinct differences. Scanning the perfect surface (Fig. 1(b)) with the 2×2 iron flat tip (Fig. 2(c)) produces images shown in Fig. 7. It is surprising to see that for the perfect surface the flat tip gives almost the same images as the pyramid tip (cf. Fig. 5). At any of these three tip-sample distances the atom positions are identifiable, although, as in the case of the pyramid geometry, contrast inversion occurs twice as tip-sample distance increases.

An interesting feature of this flat tip is observed when the surface is not perfect. Figure 8 shows a point defect surface (Fig. 1(c)) scanned with the 2×2 flat iron tip. In the repulsive force image (Fig. 8(a)) it is noted that the atom shapes are somewhat deformed around the point defect, and the forces are weak in the atom-deformed region centered around the point defect, whose size is about the size of the tip apex. This phenomenon have also been noted in an AFM simulation by Koutsos *et al.*[19] using an fcc (111) tip and an fcc (111) sample in the repulsive force range of an L–J potential. The attractive force images ((b) and (c)) also show dark (weak force) regions centered around the point defect. This observation also holds for the flat diamond tip geometry (Fig. 2(d)), in which case hexagonal mirror images of the tip apex are observed. Thus the present simulation and available

literature indicate that this phenomenon is rather universal, appearing in attractive as well as repulsive force ranges, for various tip-sample registry combinations and atomic potentials. It is also noted that with the Morse parameters used in our previous paper[23] (see above), the appearance of a false atom at the point defect is also observed.

Let us consider the reason for the above "mirroring" of the tip apex by the point defect. We note that in scanning probe microscopes such as STM and AFM, there exists no essential difference between the tip and the sample. In effect, whichever is sharper works as the tip, and the other as the sample. Thus if a rather dull tip and a surface with sharp spikes are used, mirroring of the tip onto the sample surface image is obtained. The present simulation indicates that this also happens with a sharp "dent": a point defect acts in such a case as a "negative" tip.

With the above results for the point defect surface, it becomes obvious that the flat tips are not providing "true" atomic images at any tip-sample distance. At a repulsive force distance, each tip apex atom facing the sample surface feels a force from the nearest sample atom most strongly, and the total force acting on the tip is the composite of the forces acting on each tip atom. Thus an image of one strong force point is not formed by the force exerted by only one atom, and the exact correspondence of the atom positions between the sample surface and its force image without phase shift is coincidental.

The above case is similar to the multitip effect as it may happen with soft, layered samples. In accordance with the argument of Binnig[3] and Koutsos *et al.*,[19] the above result indicates that such multitip reproduces the sample surface periodicity, with or without phase shift, as long as the surface lattice is perfect. This confirms the argument by Binnig[3] that when we see perfect periodic images, as we very often do with AFM, we do not know whether we have "true" atomic resolution or not.

These discussions also confirm the argument of Ohnesorge and Binnig[4] that the surface point defect is a good test structure for a "single atom" (single atom protruding at the apex) tip. We propose here the use of the above tip "mirror" image produced by the surface point defect for tip apex evaluation. In the present study which uses a Morse potential, the effect of the second atomic layer in the tip on AFM images is secondary, and thus this method would give approximately the size and the shape of the first atomic layer at the tip apex. This may not be true for systems whose potential is very different from the one examined here. Nevertheless, considering the fact that there exists no method of AFM tip evaluation on the atomic scale at present, this possibility may have great practical importance.

The aforementioned phase shift may happen depending on the tip-sample distance and the registry of the tip apex. An example of the former is found in Fig. 7(b), which shows half a periodicity shift both in the x and y directions. An example of the latter is shown in Fig. 9, in which the images taken with a diamond flat tip (Fig. 2(d)) are compared. Here exact atom positions are marked by open circles, and it is apparent that while

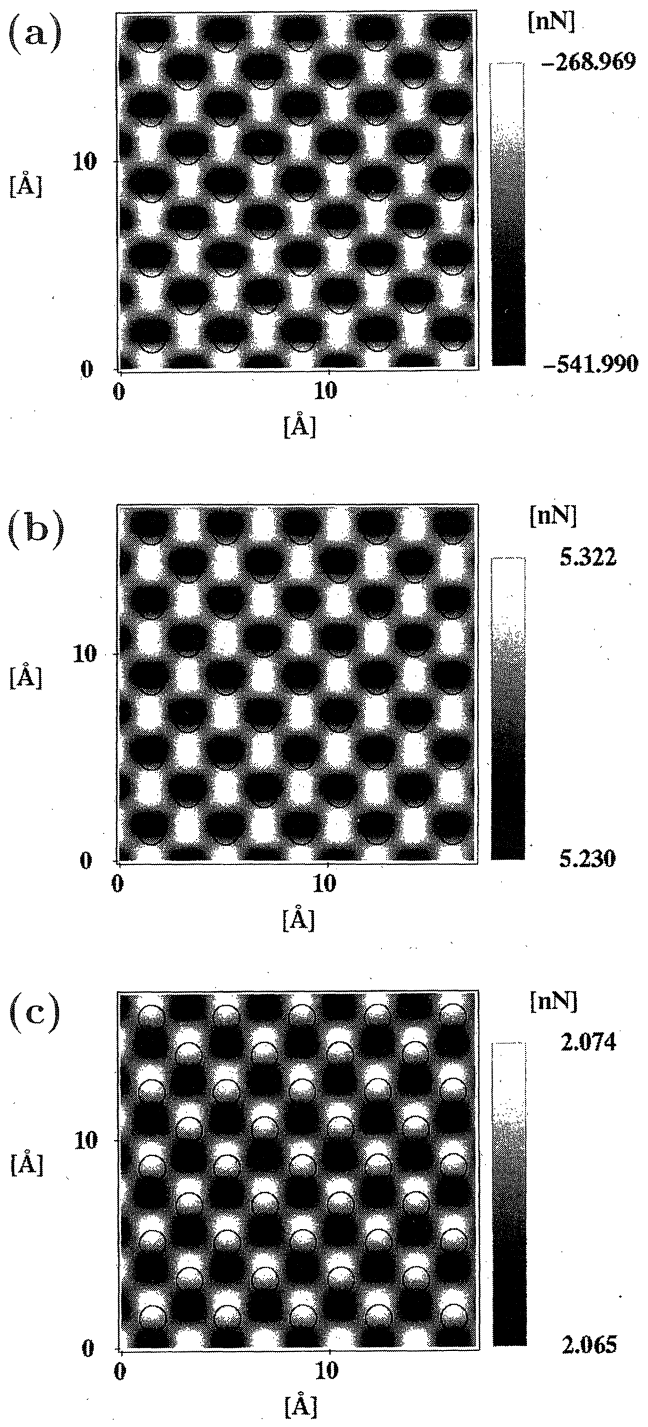

Fig. 9. The model sample surface of perfect lattice (Fig. 1(b)) as scanned with a flat diamond tip. Tip is at (a) repulsive, (b) strongly attractive and (c) weakly attractive force distance.

the obtained images give lattice periodicity corresponding exactly to that of the sample surface, the "atom" images are shifted by about quarter of a period in the y direction. This shift is apparently due to the asymmetry in the second atomic layer of the tip relative to the symmetry axis of the first atomic layer. Thus the force centers of the first and the second atomic layers do not correspond, and their superposition results in the phase shift observed in Fig. 9.

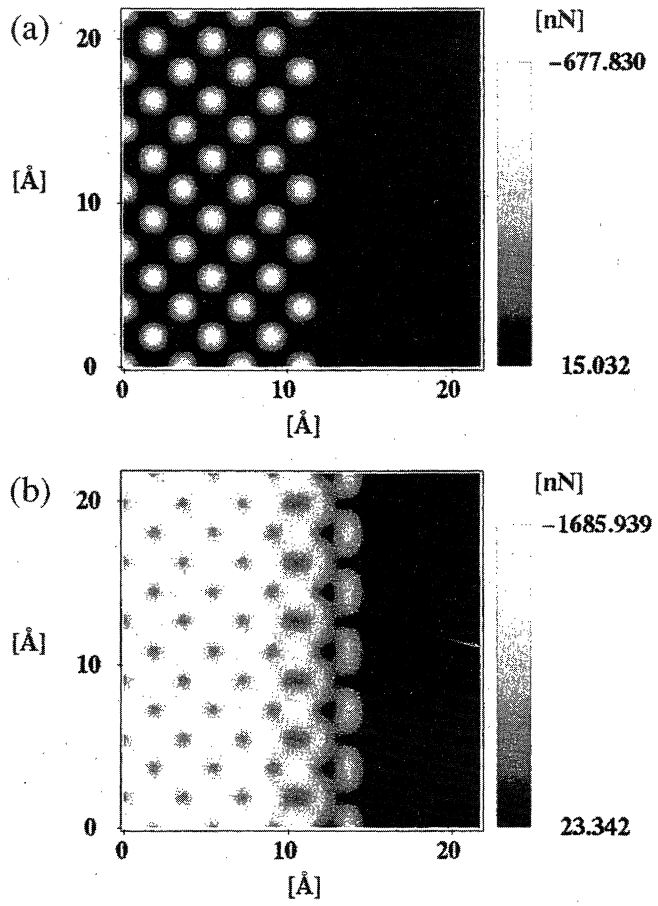

Fig. 10. Constant-height AFM images of a stepped surface (Fig. 1(d)) simulated using a single atom iron tip (a) and a flat iron tip (b) at a repulsive force distance.

3.5 *Stepped surface*

Ohnesorge and Binnig[4] mentioned that, in addition to the surface point defects, surface steps may also be good test structures for the "single atom" tip. Figure 10 compares the images of a surface with a monoatomic step (Fig. 1(d)) taken with iron pyramid and flat tips (Figs. 2(a) and 2(b)) at a repulsive force distance. While the former clearly resolves the step position and the atoms on the upper terrace (since the image is taken in the constant-height mode with no z-position feedback, atom images in the lower terrace are blacked out), the latter shows gradual geometry changes around the step position and false atomic images.

4. Conclusions

Using a newly developed AFM simulator ACCESS, AFM image variations along the surface normal were examined as a function of tip geometry. Within the framework of the present calculations, it was found that the second atomic layer of the tip also participates in AFM imaging: it influences the force characteristics of the system, and may also cause a phase shift when the symmetry axes of the first and the second atomic layers of the tip do not coincide. It is essential to have a "single-atom" tip (a tip with an atom protruding at the apex) in order to obtain atomically resolved AFM images. A tip apex evaluation method utilizing the fact that a surface point defect mirrors the atomic arrangements of the tip apex is proposed.

Acknowledgement

This work is supported in part by the Foundation for Promotion of Material Science and Technology of Japan.

1) G. Binnig, C. F. Quate and C. Gerber: Phys. Rev. Lett. **56** (1986) 930.
2) T. R. Albrecht and C. F. Quate: J. Appl. Phys. **62** (1987) 2599.
3) G. Binnig: Ultramicroscopy **42–44** (1992) 7.
4) F. Ohnesorge and G. Binnig: Science **260** (1993) 1451.
5) U. Hartman: Ultramicroscopy **42–44** (1992) 59.
6) U. Landman, W. D. Luedtke and A. Nitzan: Surf. Sci. **210** (1989) L177.
7) U. Landman, W. D. Luedtke, N. A. Burham and R. J. Colton: Science **248** (1990) 454.
8) U. Landman and W. D. Luedtke: J. Vac. Sci. Technol. B **9** (1991) 414.
9) G. Bozzoro and J. Ferrante: Ultramicroscopy **42–44** (1992) 55.
10) F. Gautier, H. Ness and D. Staeffler: Ultramicroscopy **42–44** (1992) 91.
11) U. Landman, W. D. Luedtke, J. Ouyang and T. K. Xia: Jpn. J. Appl. Phys. **32** (1993) 1444.
12) O. Tomagnini, F. Elcolessi and E. Tossati: Surf. Sci. **287/288** (1993) 1041.
13) I. Yu. Sokolov: Surf. Sci. **311** (1994) 287.
14) A. L. Shluger, A. L. Rohl, D. H. Gay and R. T. Williams: J. Phys.: Condens. Matter **6** (1994) 1825.
15) A. L. Shluger, R. M. Willson and R. T. Williams: Phys. Rev. B **49** (1994) 4915.
16) F. F. Abraham, I. P. Batra and S. Ciraci: Phys. Rev. Lett. **60** (1988) 1314.
17) C. Girard, D. Van Labeke and J. M. Vigoureux: Phys. Rev. B **40** (1989) 12133.
18) H. Tang, C. Joachim, J. Devillers: Surf. Sci. **291** (1993) 439.
19) V. Koutsos, E. Manias, G. ten Brinke and G. Hadziioannou: Europhys. Lett. **26** (1994) 103.
20) H. Tang, C. Joachim, J. Devillers and C. Girard: Europhys. Lett. **27** (1994) 383.
21) N. Sasaki and M. Tsukada: Jpn. J. Appl. Phys. **34** (1995) 3319.
22) N. Sasaki and M. Tsukada: Phys. Rev. B **52** (1995) 8471.
23) M. Komiyama, K. Tsujimichi, S. Ohkubo, K. Tazawa, M. Kubo and A. Miyamoto: Jpn. J. Appl. Phys. **34** (1995) L789.
24) M. Komiyama, K. Tazawa, K. Tsujimichi, A. Hirotani, M. Kubo and A. Miyamoto: to be published in Thin Solid Films.
25) M. Komiyama, K. Tsujimichi, K. Tazawa, A. Hirotani, H. Yamano, M. Kubo, E. Broclawik and A. Miyamoto: to be published in Surf. Sci.
26) L. A. Girifalco and V. G. Weizer: Phys. Rev. **114** (1959) 687.